Cellulose (2023) 30:8405–8413
https://doi.org/10.1007/s10570-023-05388-1

ORIGINAL RESEARCH

Mesostructural changes in cellulose within wood cell wall upon hydrothermal treatment at 200 °C

Tomoko Kuribayashi · Yu Ogawa · Isabelle Morfin · Yuji Matsumoto · Yoshiharu Nishiyama

Received: 17 May 2023 / Accepted: 10 July 2023 / Published online: 9 August 2023

Abstract Hydrothermal treatment between 150 °C and 230 °C is widely used in wood processing, from the steam treatment of timber for better dimensional stability and durability to the pretreatment for enzymatic saccharification and chemical pulping. Understanding the ultrastructural changes of wood cell walls through hydrothermal treatments is crucial for controlling and optimizing these hydrothermal treatment-based processes. Here, we studied the ultrastructure of wood cell walls of 24 hardwood species using simultaneous small- and wide-angle X-ray scattering measurements before and after the hydrothermal treatment at 200 °C. Most hardwoods show similar equatorial scattering features, representing the structure in the cross-section of the cell walls. In a water-saturated native state, there is a prominent correlation peak between 0.1 and 0.2 $Å^{-1}$ and a second peak between 0.2 and 0.4 $Å^{-1}$. The hydrothermal treatment above 160 ˚C drastically altered the structure at this nanometric scale: the two native correlation peaks disappeared, coincident with a buildup of a correlation peak in the 0.03–0.04 $Å^{-1}$ range. The hydrothermal treatment likely removed the cell wall matrix component between the microfibrils through autohydrolysis and phase separation, leading to the collapse of microfibrils with each other in the normal wood. In cellulose-rich cell walls, such as the G-layer in tension wood, cellulose microfibrils are already collated in the native state.

Keywords Wood · Cellulose microfibril · Mesostructure · X-ray scattering · Hydrothermal treatment · Co-crystallization

Supplementary Information The online version contains supplementary material available at https://doi.org/10.1007/s10570-023-05388-1.

T. Kuribayashi (✉) · Y. Matsumoto
Department of Biomaterials Science, Graduate School of Agricultural and Life Sciences, The University of Tokyo, Yayoi 1-1-1, Bunkyo-Ku, Tokyo 113-8657, Japan
e-mail: tomoko.kuribayashi@aalto.fi

T. Kuribayashi
Department of Bioproducts and Biosystems, Aalto University, Vuorimiehentie 1, 02150 Espoo, Finland

T. Kuribayashi
Department of Food and Nutrition, University of Helsinki, P.O. Box 66, 00014 Helsinki, Finland

Y. Ogawa · Y. Nishiyama
Univ. Grenoble Alpes, CNRS, CERMAV, 38000 Grenoble, France
e-mail: yoshiharu.nishiyama@cermav.cnrs.fr

I. Morfin
Univ. Grenoble Alpes, CNRS, LiPhy, 38000 Grenoble, France

Introduction

Thermal treatment between 150 °C and 230 °C with moisture is commonly used in timber processing.

Heat steam treatment decreases wood's equilibrium moisture content, improving dimensional stability and durability (Kocaefe et al. 2015; Sandberg and Kutnar 2016). Hydrothermal treatment with excess water causes partial hydrolysis of the hemicelluloses that generates water-soluble saccharides and increases the specific surface area of the wood (Garrote et al. 1999). Such effects are helpful in the pretreatment of woody biomass for saccharification and chemical pulping (Garrote et al. 1999; Nitsos et al. 2013, 2016; Romani et al. 2010; Wojtasz-Mucha et al. 2017). The ultrastructural changes of wood cell walls by hydrothermal treatments are thus an important parameter.

X-ray scattering can probe the structural features over wide length scales, typically from angstroms to a few hundred nanometers, without special sample preparation, which makes it a suitable analytical tool for structural investigations of plant cell walls (Jakob et al. 1994, 1996; Fernandes et al. 2011; Penttilä et al. 2019). Small- (SAXS) and wide-angle X-ray scattering (WAXS) have been used to study the structural evolutions of fully hydrated aspen (Nishiyama et al. 2014) and bagasse (Driemeier et al. 2015) during hydrothermal treatments. These studies found several common structural changes, such as co-crystallization of cellulose and phase separation of the cell wall matrix component (Nishiyama et al. 2014; Kuribayashi et al. 2016). We extended this study to broader spectrum wood samples, including 24 hardwood species before and after hydrothermal treatment at 200 °C for 2 h using simultaneous S/WAXS measurements.

Experimental

Materials

Green beech (*Fagus crenata*) was harvested from The University of Tokyo Chichibu Forest (Saitama, Japan). Blocks (dimensions: 13 mm × 13 mm × 60 mm in the direction of tangential (T), radial (R), and longitudinal (L), respectively) were sawn out from the mature sapwood and stored in water with sodium azide at 4 °C.

Air-dried 24 hardwood specimens are summarized in Table 1. These were harvested in Japan and kindly provided by the Research Institute for Sustainable Humanosphere (RISH), Kyoto University, Japan.

Table 1 A list of wood specimens and their moisture contents

No.	Scientific name	Common name	Mc [%] [a]		
			Air dry	Wet	
			Untreated	Untreated	Thermal treated
1	*Acer* sp.	Maple	7	121	123
2	*Aesculus turbinata*	Japanese horse-chestnut	8	123	128
3	*Aphananthe aspera*	Muku tree	8	82	87
4	*Castanea crenata*	Japanese chestnut	8	117	110
5	*Castanopsis* sp.	Chinquapin	8	116	105
6	*Celtis sinensis*	Chinese hackberry[b]	7	142	130
7	*Cercidiphyllum japonicum*	Katsura	7	139	139
8	*Cinnamomum camphora*	Camphor tree	7	108	128
9	*Cleyera japonica*	Japanese cleyra	6	187	183
10	*Diospyros kaki*	Japanese persimmon	6	94	97
11	*Distylium racemosum*	Isu tree	10	98	97
12	*Firmiana simplex*	Chinese parasol tree	7	90	86
13	*Fraxinus mandshurica*	Manchurian ash	6	133	149
14	*Ilex Integra*	Mochi tree	6	82	88
15	*Kalopanax septemlobus*	Castor aralia[b]	6	135	143
16	*Liriodendron tulipifera*	Yellow poplar	7	141	154
17	*Magnolia obovata*	Japanese bigleaf magnolia	9	114	148
18	*Morus* sp.	Mulberry	7	135	130
19	*Quercus* sp.	Oak	9	110	83
20	*Quercus acutissima*	Sawtooth oak	9	85	83

No.	Scientific name	Common name	Mc [%] [a]		
			Air dry	Wet	
			Untreated	Untreated	Thermal treated
21	*Quercus crispula*	Mizunara	7	100	97
22	*Styphnolobium japonicum*	Japanese pagoda tree	6	96	98
23	*Ulmus davidiana*	David elm	8	193	209
24	*Zelkova serrata*	Japanese elm	9	120	116

[a] Mc [%] = Dry basis moisture content

[b] Tension wood

Preparation of water-swollen wood samples

Cylindrical samples with about 2 mm diameter and 10 mm length in fiber direction were cut out from the air-dried wood blocks. Specimens were cropped from the part without visible large vessel pores and medullary rays. Deionized water was soaked in the samples by vacuum pressure impregnation until the sample weight did not increase. The dry-basis moisture content of water-saturated samples was estimated as follows. A part of air-dried samples was dried overnight in an oven at 105 °C to obtain the dry weight. We calculated the equilibrium moisture contents of water-saturated samples in the ambient condition and considered it to be the same for each wood species. Moisture contents in the water saturated samples were estimated taking into account the equilibrium moisture contents and weight gain by water impregnation. The calculated moisture contents in air-dried and water-saturated states were summarized in Table 1. Immediately after weighing the water-saturated sample, each wet sample was sealed into a glass tube (3 mm outer diameter, 200 µm wall thickness).

Hydrothermal treatment

The glass tubes containing a wood sample and a drop of water for pressure regulation were placed in a 30 ml pressure vessel and heat-treated in an oil bath at 200 °C for 2 h. The partial water vapor pressure during hydrothermal treatment is 1.6 MPa according to the Tetens approximation formula. After the treatment, the vessel was quenched with ice.

Simultaneous SAXS and WAXS measurement

X-ray scattering experiments were performed at the D2AM beamline of the European Synchrotron Radiation Facility (ESRF). The tubes containing samples were probed with a monochromatic X-ray of 18 keV ($\lambda = 0.6889$ Å) before and after the hydrothermal treatment. The incident beam was orthogonal to the sample tubes. The scattering intensity was measured using two-dimensional pixel detection (XPAD-WOS and D5). Two sets of camera distances, D5 at 2.2 m and WOS at 32 cm, and D5 at 1 m and WOS at 12 cm were used to cover a scattering vector range of q ($2\pi/d$) = 0.005 to 6 $Å^{-1}$ (0.13 µm to 1 Å in real space).

In-situ X-ray scattering measurement over the thermal treatment

We used an aluminum block with 3 mm perforations to fit sample tubes and holes for incoming X-rays and scattered X-rays at D2AM beamline (ESRF). The temperature was regulated by using a heater regulated by a Eurotherm temperature controller. Sample tubes containing green wood and wood with moisture content of 0–30% were sealed by flame and placed in the sample holder. The samples were first heated from 25 °C to 80 °C, and the temperature was elevated stepwise by 10 °C with 10 min of holding time. After reaching 200 °C, the temperature was kept for 2 h, then cooled to 23 °C by heat dissipation. The X-ray energy was 16 keV ($\lambda = 0.775$ Å). The scattered X-rays were recorded on a fiber optic coupled CCD camera. The experiment was repeated twice with two detector distances, 1.6 m and 16 cm, to cover a q range from 0.03 to 2 $Å^{-1}$.

Data analysis

The beam center and the detector positions were refined using PyFAI (Ashiotis et al. 2015) software using silver behenate and Chromium(III)

oxide diluted with microcrystalline cellulose powder in the same sample tube as the calibrant. The data were scaled by transmission intensity and remapped into polar coordinates. The intensity of the overlapping region was used to scale the two data sets measured at different detector distances and merged into one figure. The isotropic scattering level was estimated for each scattering angle by averaging 10% of pixels of the lowest intensities. For the in-situ experiment data, the azimuthal intensity distributions were fitted with a constant and a Gaussian function for each scattering angle to separate the isotropic and the equatorial (anisotropic) contributions (Nishiyama et al. 2014).

Results and discussion

Changes in the scattering profile of anisotropic components

Examples of scattering patterns obtained from *Quercus* sp. are shown in Fig. 1. The untreated and treated wood show anisotropic scattering features over the whole q range: SAXS-1 and 2 show a streak in the equatorial direction (Fig. 1a), while WAXS-1 and 2 show fiber diffraction patterns where cellulose is oriented along the long axis of wood (Fig. 1b). The scattering profile of equatorial components of *Quercus* sp. is shown in Fig. 1c, where $q \times I$ is plotted as a function of q, where I is an intensity count at a given q. Multiplying by q is equivalent to making an abstraction of the misalignment of cylindrically symmetric structure and extracting the power spectrum of the electron density of the cross-section.

In the WAXS range, a composite peak of 1 -1 0/1 1 0 reflections and the 2 0 0 reflections of cellulose Iβ are visible at 1.1 and 1.6 $Å^{-1}$, respectively. The pattern before the thermal treatment (blue profile) is typical of wood samples, and the positions and the intensity ratio roughly correspond to those obtained from highly crystalline cellulose Iβ. After hydrothermal treatment at 200 °C, the equatorial reflections became much sharper due to the co-crystallization of microfibrils as reported previously (Fig. 1a and b) (Kuribayashi et al. 2016, 2019).

In the lower q range recorded, two peaks are present at $q = 0.1–0.2$ $Å^{-1}$ and $q = 0.3–0.4$ $Å^{-1}$ in the untreated sample (Fig. 1a). Several studies have previously observed the former peak using X-ray (Jakob et al. 1996; Chen et al. 2021; Paajanen et al. 2022) or neutron (Fernandes et al. 2011; Nishiyama et al. 2014). The peak can be explained by the correlation between hard cylinders (i.e. cellulose microfibrils) randomly packed in the cell wall (Jakob et al. 1996) or the center-to-center distance of cylinders (Fernandes et al. 2011) or the convolution of the form factor of cylindrical microfibrils and their correlation (Chen et al. 2021). The latter peak has not been clearly explained, while Viljanen and co-workers (2020) reported a peak fitting of the peak observed in a SAXS profile of a tropical wood using a form factor of a cylinder. In Paajanen et al. (2022), the sample volume in the beam was probably too small compared to the Kapton window film whose scattering overlapped with this peak. In Jakob et al. (1996), the part of the peak can be recognized, but the limited q-range did not allow the appreciation of the whole feature. In our study, we used a sample thickness of about 2.5 mm, leading to sufficiently high scattering intensity with respect to the contribution of optical elements in the beam, revealing that this peak is another common scattering feature of many hardwood species.

The hydrothermal treatment drastically changed the scattering features: the 0.3 $Å^{-1}$ and the 0.15 $Å^{-1}$ peaks completely disappeared, and a new peak appeared at a much lower q range (0.01- 0.05 $Å^{-1}$). The streak intensities increased in the q range of 0.06–0.6 $Å^{-1}$. Below $q = 0.01$ $Å^{-1}$, the intensity decay followed a power law. We carried out the same hydrothermal treatment on the 24 species. As summarized in Fig. 2, the small angle peaks (white arrowheads in Fig. 2(b)) were visible between 0.12–0.16 A^{-1} in most wood species before the treatment except 4 species *(D. kaki*, *C. sinensis*, *K. septemlobus*, and *S. japonicum*). Similar to the case of *Quercus* sp., this peak disappeared after the thermal treatment, and the new broad peak appeared centered 0.02–0.04 A^{-1} (black arrowheads in Fig. 2b). This change indicates that the hydrothermal treatment commonly induced the structural coarsening of approximately one order of magnitude in length scale in the cell walls of these 20 species.

On the other hand, the above-mentioned 4 species had small-angle peaks at 0.03 A^{-1} before the hydrothermal treatment (Fig. 2a). While the peak intensities increased, the peak positions remained at

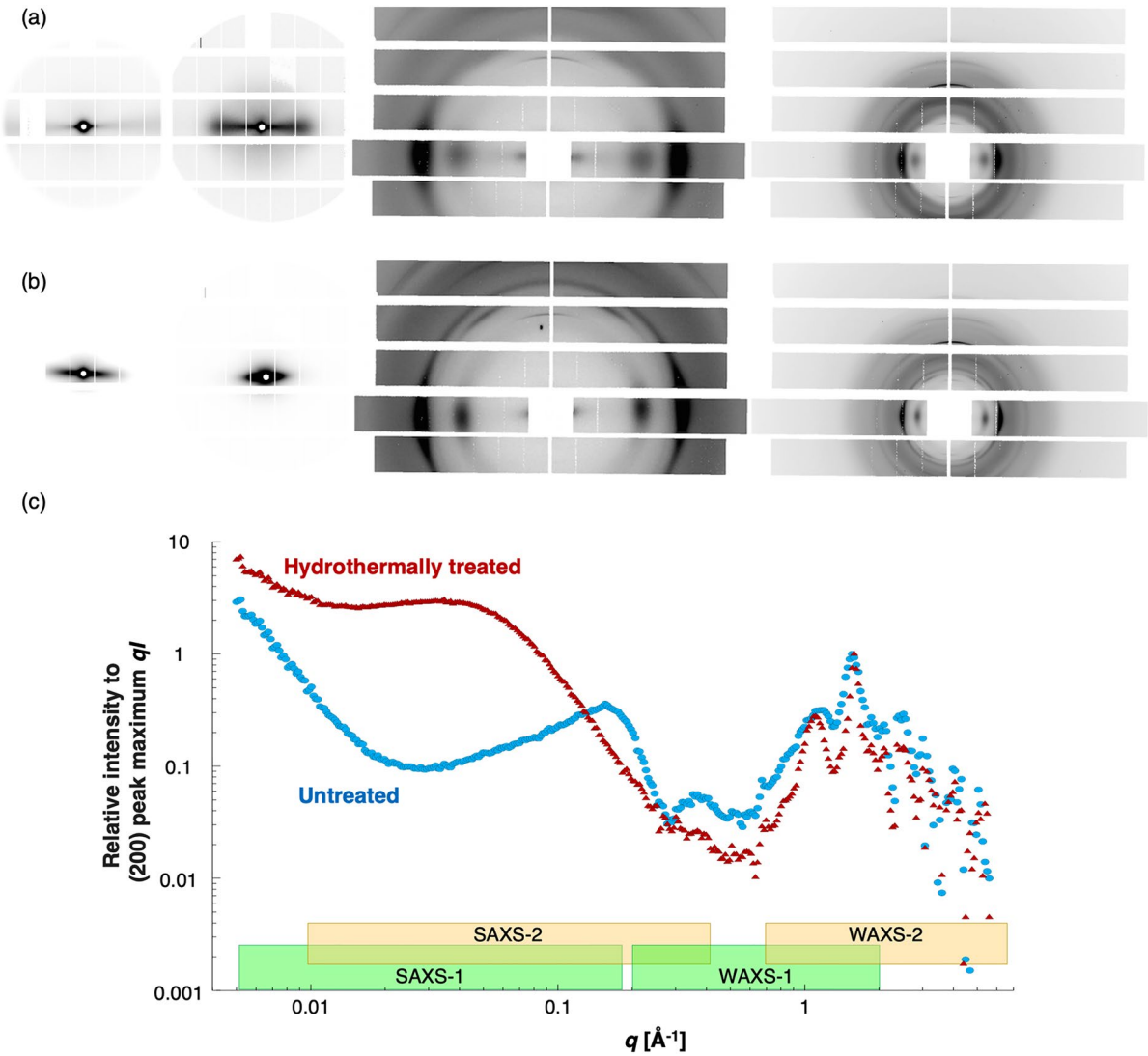

Fig. 1 Two-dimensional scattering images **a**, **b** and profiles of equatorial component **c** of the wet oak wood sample (*Quercus* sp.) before **a** and blue profile in **c** and after hydrothermal treatment at 200 °C for 2 h **b** and red profile in **c**. Scattering images in **a** and **b** are SAXS-1, SAXS-2, WAXS-1, and WAXS-2 from left to right. The X-ray beam was irradiated orthogonal to the wood fiber direction (i.e., the fiber direction was vertical in the diagrams)

the same positions after the treatment of these species (Fig. 2b). Thus, the hydrothermal treatment did not strongly affect the structural features at this ten-nanometer length scale related to the organization of cellulose microfibrils in the cell walls. Optical micrographs of *C. sinensis* (6), *K. septemlobus* (15) before the treatment show thick G-layers in the fiber cells (Fig. S1). The G-layer is a non-lignified cell wall layer composed mostly of cellulose. The lack of the matrix components in the G-layer may cause the coalescence of cellulose microfibrils, similarly in the hydrothermally treated cell walls, resulting in a coarse cell wall structure and hence similar scattering features before and after the treatment. The other two species, *D. kaki* (10), *S. japonicum* (22), as well as the remaining 22 specimens, did not show G-layer in

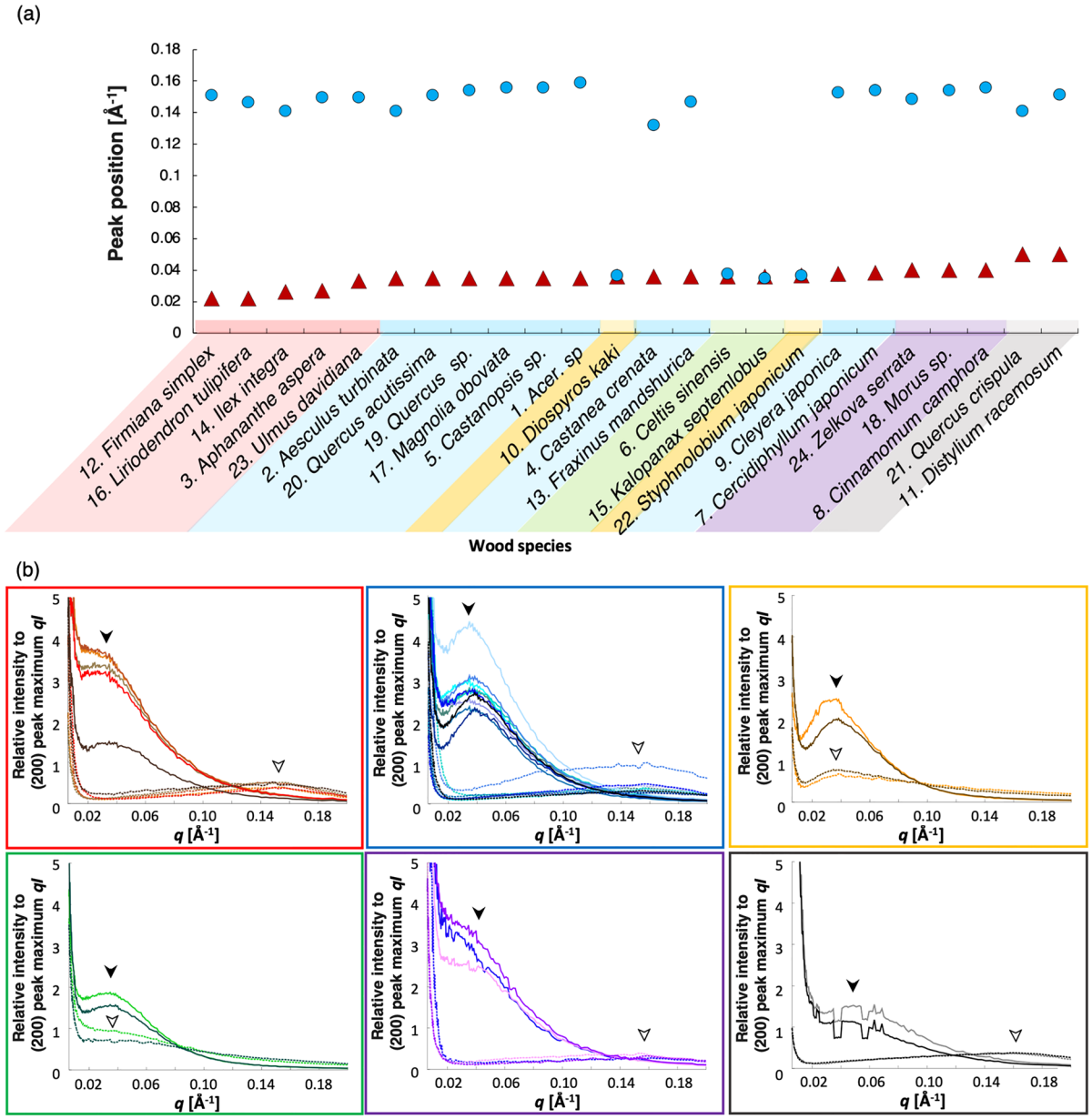

Fig. 2 **a** Peak positions of prominent correlation peaks of 24 wood species before (blue circle) and after the hydrothermal treatment (red triangle). **b** Corresponding X-ray scattering profiles before (dotted lines) and after the hydrothermal treatment (solid lines) in the double linear scale. The line colors in **b** correspond to those in **a**

their micrographs, while the scattering patterns were similar to the aforementioned species with the tension wood feature (Fig. S1). The solid-state ^{13}C NMR analysis suggested that specimens of *C. sinensis* (6), *K. septemlobus* (15), *D. kaki* (10) contained a higher amount of crystalline cellulose compared to other specimens (Kuribayashi et al. 2019).

Q range below 0.01 Å^{-1}

In the smaller angle region below 0.01 A^{-1}, power-law behavior can be seen after hydrothermal treatment, as shown in Fig. 3. The straight line extends to q = 0.4 Å^{-1} in 21 species, as seen in the double logarithmic scale. The slope constants were between -1.3

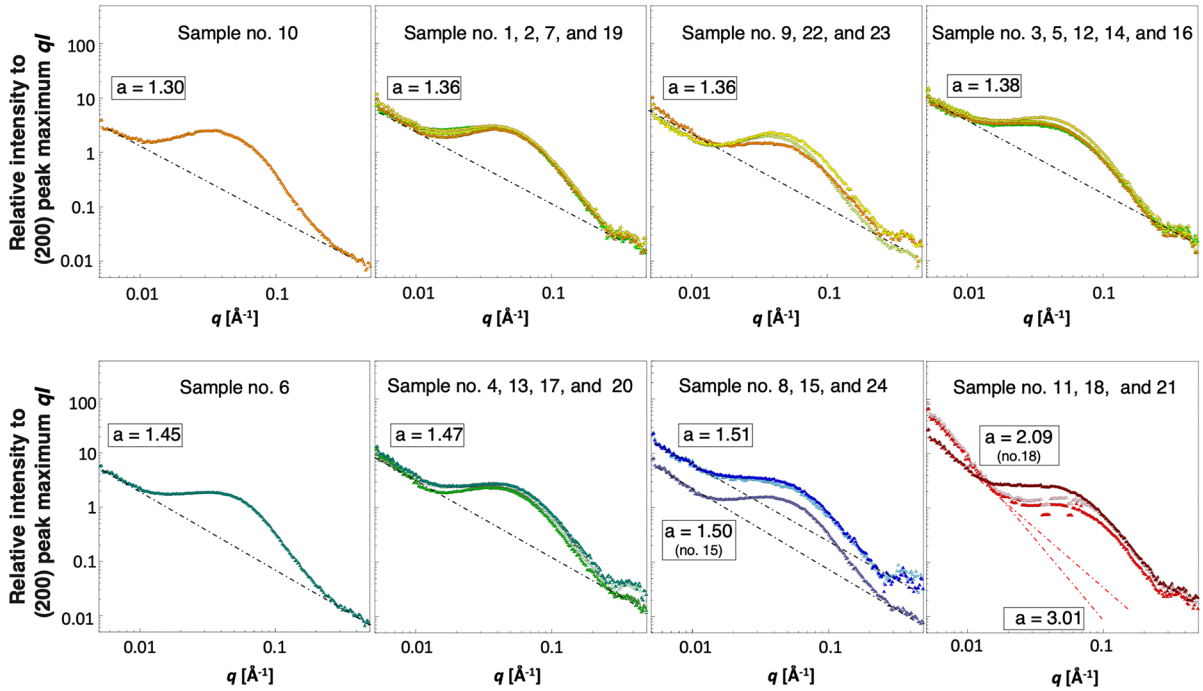

Fig. 3 Scattering profiles of 24 hydrothermally treated wood species between q = 0.006 and 0.3 $Å^{-1}$ in double log scale with power-law slopes as dotted lines **a**. Numbers correspond to those in Table 1

to -1.5. The remaining 3 species, *D. racemosum* (11), *Morus* sp. (18), *Q. crispula* (21), show higher exponents in the low q range below 0.01 A^{-1}. In particular, the constants for *D. racemosum* and *Q. crispula* are -3, corresponding to the presence of a clear interface in the structure. This might be due to air bubbles in the specimens, resulting in the air–solid interfaces.

The relationship between the slope constants and the peak positions after the hydrothermal treatment is shown in Fig. 4. Among 24 species studied in this study, 17 of them show a notable similarity in these two scattering features in the small angle regions, with the power-low exponent of about -1.4 and the peak positions at 0.032 to 0.04 A^{-1}. Despite the taxonomical and ultrastructural differences found before the treatment, the hydrothermal treatment at 200 °C converges to a similar structure in the cell wall at a nanometric length scale.

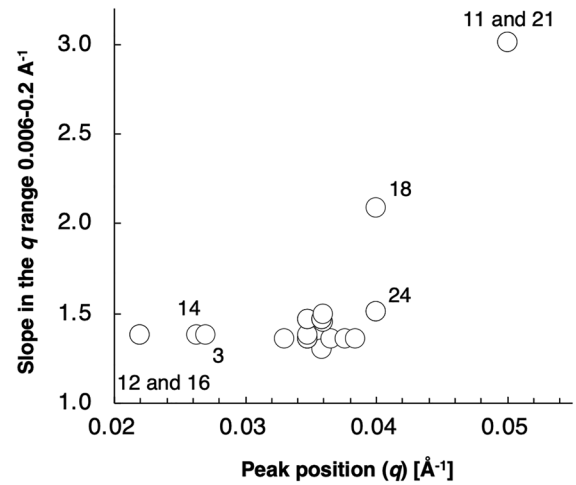

Fig. 4 Relationship between power-law slope constants and peak positions of the main correlation peak of 24 wood species after hydrothermal treatment. Numbers correspond to those in Table 1

Structural changes during the in-situ experiment

To follow the structural changes due to the hydrothermal treatment, we performed in situ S/WAXS measurements during the hydrothermal treatment of beech wood (*Fagus crenata*) at 200 °C, as shown in Fig. 5. This series of the equatorial scattering profiles indicates that these changes occurred only in the water-saturated

sample but not in the air-dried sample (Fig. 5a and b). All the major structural changes happened during the heating process, and the cooling did not affect the structure. The increase in the streak intensity at $q < 0.2$ Å^{-1} started at 160 °C. Fig. S1(a)). The 0.3-Å^{-1} peak weakened and eventually disappeared during the heating from 130˚C to 150˚C. The 0.15-Å^{-1} peak also disappeared during the heating, where the intensity weakening started at around 160 ˚C. This temperature range of around 160 ˚C is typically the onset of autohydrolysis of hemicelluloses (Santucci et al. 2015). Thus, the loss of the 0.15 Å^{-1} peak may originate from the collapse of cellulose microfibrils induced by removing hemicelluloses from the interfibrillar space. This possible mechanism also explains the less pronounced structural change in the air-dried sample, as the extensive autohydrolysis requires excess water in the system.

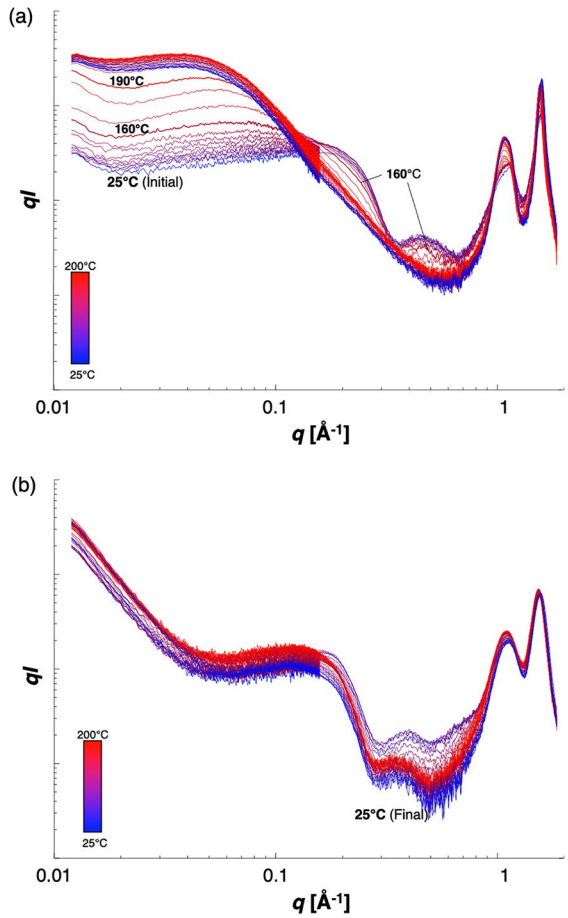

Fig. 5 In situ S/WAXS profiles of the equatorial component during hydrothermal treatment. Green (a) and air-dry (b) beech wood (*F. crenata*)

Conclusion

This study investigated cellulose structural changes over a wide length scale from a scale of interplanar spacing of cellulose crystal (a few angstroms) to that close to the thickness of secondary cell wall sublayers (a few hundred nanometers). Most hardwoods show similar equatorial scattering features that represent the structure in the cross-section of the cell wall, in the q range spanning 3 decades between 0.005 and 6 Å^{-1}. In a water-swollen native state, there is a prominent correlation peak between 0.1 and 0.2 Å^{-1} and a second peak between 0.2 and 0.4 Å^{-1}. These correlation peaks disappear upon hydrothermal treatment above 160˚C, accompanied by a buildup of a correlation peak in the 0.03–0.04 Å^{-1} range. Some exceptions were seen in cellulose-rich samples, where the correlation peaks between 0.1 and 0.4 Å^{-1} are absent in the native state. The hydrothermal treatment is probably leaching out the matrix component between the microfibrils leading to the collapse of microfibrils with each other in the normal wood. In contrast, cellulose microfibrils are already collapsed to each other in the native state in cellulose-rich cell walls.

Acknowledgments This study was supported by JSPS KAKENHI Grant Number JP17J05156 (T.K.). The dried wood specimens were obtained through collaborative research using wood collection databases with Research Institute for Sustainable Humanosphere (RISH) (Y.M. and T.K.). We thank Prof. Junji Sugiyama and Hajime Sorimachi (Kyoto University, Japan) for advising us on the selection of wood specimens. We thank the support of Prof. Yukie Saito (The University of Tokyo, Japan) and The University of Tokyo Chichibu Forest and Arboricultural Research Institute (UTCF) during the sampling of beech green wood specimens. We acknowledge Glyco@Alps (ANR-15-IDEX-02) for the financial support. The wide-angle X-ray detector (WOS) was funded by the French National Research Agency (ANR) under the 'Investissement d'Avenir' program (Grant No. ANR-11-EQPX-0010). ESRF is acknowledged for the provision of beamtimes (experiment numbers A02-1-892 and A02-1-864, D2AM beamline).

Author contributions TK, YO, and YN conceptualized the study. TK, YO, IM, and YN performed the experiments. TK, YO, and YN analyzed the data. TK, YO, and YN wrote the manuscript. YM and YN supervised the study. All authors read and approved the final manuscript.

Funding Open Access funding provided by Aalto University.

Data availability All data generated or analyzed during this study are included in this article and the supporting information file.

Declarations

Conflict of interest The authors have no relevant financial or non-financial interests to disclose.

Consent for publication All authors have provided their consent for publication.

Ethical approval and consent to participate Not applicable.

References

Kuribayashi T, Ogawa Y, Rochas C, et al (2016) Hydrothermal Transformation of Wood Cellulose Crystals into Pseudo-Orthorhombic Structure by Cocrystallization. ACS Macro Lett 5:730–734. https://doi.org/10.1021/acsmacrolett.6b00273

Ashiotis G, Deschildre A, Nawaz Z et al (2015) The fast azimuthal integration Python library: pyFAI. J Appl Crystallogr 48:510–519. https://doi.org/10.1107/S1600576715004306

Chen P, Li Y, Nishiyama Y et al (2021) Small Angle Neutron Scattering Shows Nanoscale PMMA Distribution in Transparent Wood Biocomposites. Nano Lett 21:2883–2890. https://doi.org/10.1021/acs.nanolett.0c05038

Driemeier C, Mendes FM, Santucci BS, Pimenta MTB (2015) Cellulose co-crystallization and related phenomena occurring in hydrothermal treatment of sugarcane bagasse. Cellulose 22:2183–2195. https://doi.org/10.1007/s10570-015-0638-7

Fernandes AN, Thomas LH, Altaner CM et al (2011) Nanostructure of cellulose microfibrils in spruce wood. Proc Natl Acad Sci 108:E1195–E1203. https://doi.org/10.1073/pnas.1108942108

Garrote G, Domínguez H, Parajó JC (1999) Hydrothermal processing of lignocellulosic materials. Holz Als Roh - Und Werkst 57:191–202. https://doi.org/10.1007/s001070050039

Jakob HF, Fratzl P, Tschegg SE (1994) Size and Arrangement of Elementary Cellulose Fibrils in Wood Cells: A Small-Angle X-Ray Scattering Study of Picea abies. J Struct Biol 113:13–22. https://doi.org/10.1006/jsbi.1994.1028

Jakob HF, Tschegg SE, Fratzl P (1996) Hydration Dependence of the Wood-Cell Wall Structure in Picea abies. A Small-Angle X-Ray Scattering Study Macromolecules 29:8435–8440. https://doi.org/10.1021/ma9605661

Kocaefe D, Huang X, Kocaefe Y (2015) Dimensional stabilization of wood. Curr for Reports 1:151–161. https://doi.org/10.1007/s40725-015-0017-5

Kuribayashi T, Ogawa Y, Matsumoto, et al (2019) Changes in Crystal Structure of Cellulose in Hardwood Cell Walls by Hydrothermal Treatment at 200 °C under 1.6 Mpa. Mokuzai Gakkaishi 65:212–217

Nishiyama Y, Langan P, O'Neill H et al (2014) Structural coarsening of aspen wood by hydrothermal pretreatment monitored by small- and wide-angle scattering of X-rays and neutrons on oriented specimens. Cellulose 21:1015–1024. https://doi.org/10.1007/s10570-013-0069-2

Nitsos CK, Matis KA, Triantafyllidis KS (2013) Optimization of hydrothermal pretreatment of lignocellulosic biomass in the bioethanol production process. Chemsuschem 6:110–122. https://doi.org/10.1002/cssc.201200546

Nitsos CK, Choli-Papadopoulou T, Matis KA, Triantafyllidis KS (2016) Optimization of hydrothermal pretreatment of hardwood and softwood lignocellulosic residues for selective hemicellulose recovery and improved cellulose enzymatic hydrolysis. ACS Sustain Chem Eng 4:4529–4544. https://doi.org/10.1021/acssuschemeng.6b00535

Paajanen A, Zitting A, Rautkari L, et al (2022) Nanoscale Mechanism of Moisture-Induced Swelling in Wood Microfibril Bundles. Nano Lett 22:5143–5150. https://doi.org/10.1021/acs.nanolett.2c00822

Penttilä PA, Rautkari L, Österberg M, Schweins R (2019) Small-angle scattering model for efficient characterization of wood nanostructure and moisture behaviour. J Appl Crystallogr 52:369–377. https://doi.org/10.1107/S1600576719002012

Romaní A, Garrote G, Alonso JL, Parajó JC (2010) Bioethanol production from hydrothermally pretreated Eucalyptus globulus wood. Bioresour Technol 101:8706–8712. https://doi.org/10.1016/j.biortech.2010.06.093

Sandberg D, Kutnar A (2016) Thermally modified timber: Recent developments in Europe and North America. Wood Fiber Sci 48:28–39

Santucci BS, Maziero P, Rabelo SC et al (2015) Autohydrolysis of Hemicelluloses from Sugarcane Bagasse During Hydrothermal Pretreatment: a Kinetic Assessment. BioEnergy Res 8:1778–1787. https://doi.org/10.1007/s12155-015-9632-z

Viljanen M, Ahvenainen P, Penttilä P, Svedström K (2020) Ultrastructural X-ray scattering studies of tropical and temperate hardwoods used as tonewoods. IAWA J 41:301–319. https://doi.org/10.1163/22941932-bja10010

Wojtasz-Mucha J, Hasani M, Theliander H (2017) Hydrothermal pretreatment of wood by mild steam explosion and hot water extraction. Bioresour Technol 241:120–126. https://doi.org/10.1016/j.biortech.2017.05.061